A Simplified DTC-SVPWM Scheme for Induction Motor Drives Using a Single PI Controller

Antony K. Peter, *Student Member, IEEE*, Jaison Mathew, *Senior Member, IEEE*, and K. Gopakumar, *Fellow, IEEE*

***Abstract*—Apart from variable switching frequency, a major issue in direct torque controlled (DTC) induction motor drives is the high torque ripple, which can be minimized by incorporating suitable pulsewidth modulation schemes such as space vector pulsewidth modulation (DTC-SVPWM) and duty ratio control DTC. However, the simplicity and robustness of the DTC scheme are compromised due to the high computational complexity and requirement of a number of motor parameters for the control. In this article, a simple and elegant control algorithm for the realisation of the DTC-SVPWM that is less dependent on motor parameters is proposed. The stator flux-linkage space vector angle needed to generate the reference torque for the DTC operation is computed based on the basic torque equation and the reference stator phase voltage needed for the SVPWM is determined in turn in every sampling period. For the modulation, a carrier-based space vector pulsewidth modulation (CSVPWM) scheme is adopted to get low torque ripple at constant switching frequency. The proposed speed control scheme avoids the use of rotor parameters and rotating reference frame transformations. It requires no sector identification and only one PI controller is needed for the speed control. Though the scheme has comparable torque ripple as that of the conventional DTC-SVPWM scheme, it significantly reduces the computational burden. Hardware results on a three-phase, 2 HP, 415 V induction motor are presented to validate the performance of the proposed control scheme.**

***Index Terms*—Direct torque control, field-oriented control, induction motor drives, pulsewidth modulation, space vector modulation.**

I. Introduction

QUICK torque response, absence of coordinate transformation, low parameter dependence, and robustness of the motor drive [1] are some of the important reasons that make direct torque control (DTC) of induction motor a popular choice in industries. However, it has quite a few important drawbacks such as high torque ripple, variable switching frequency, and requirement of high sampling rate compared to average switching frequency to get acceptable performance [2], [3]. The main reason for the high current and torque ripple can be attributed to the direct application of voltage vectors without volt-second balance. This idea has motivated many researchers to integrate DTC with space vector PWM (DTC-SVPWM), which improves the torque ripple of the drive significantly, albeit a slight reduction in the speed of response [2]–[11]. To reduce the torque ripple in DTC, a scheme with sliding mode controllers in the torque and flux channels; and a PI controller in the outer speed loop is proposed in [12]. However, the need for three controllers makes it hard to implement. In [2], [5], [6], [7], a speed controller is used to determine the reference torque, which is followed by a torque controller and a flux controller in synchronous reference frame to generate the reference voltages. The need for three controllers together with rotational coordinate transformation makes these drive scheme complex and the controller tuning challenging. In [8], [9], [10], the requirement of rotational coordinate transformation is avoided by slip speed calculation. From the slip speed, reference stator flux-linkage vector is calculated and the switching pulses are generated accordingly. However, the transient performance is compromised and the need of two PI controllers makes the tuning difficult.

In [13] and [14], a single PI controller is used to generate the reference stator flux-linkage space vector for the DTC. Though the control complexity is reduced, the control algorithm depends heavily on motor parameters such as rotor resistance and self-inductance. Moreover, the motor parameters change widely with temperature and magnetic saturation and it can lead to poor performance of the drive.

Though field-oriented control (FOC) schemes can provide better torque ripple performance than DTC, it requires rotational coordinate transformations, has inferior transient performances and is heavily dependent on machine parameters, which are not readily available from the nameplate details [15], [16], [17], [18], [19], [20], [21]. The parameter estimation can become very critical and complex in control schemes that depends heavily on motor parameters [22], [23].

Some of the recent works related to DTC schemes use predictive controller and duty ratio regulation techniques to improve the torque ripple. In [24], a predictive torque controller based on discrete space vector modulation (DSVM) was proposed, where 38 virtual vectors are generated by averaging three actual voltage vectors. In [25], a model prediction flux controller is used with a modified DSVM technique which reduces the number of virtual voltage vectors from 38 to 15. However, estimation and prediction based on cost function used in [24]

Manuscript received 15 December 2021; revised 8 June 2022; accepted 3 August 2022. Date of publication 8 August 2022; date of current version 10 October 2022. Recommended for publication by Associate Editor S.-C. Yang. *(Corresponding author: Jaison Mathew.)*

Antony K. Peter and Jaison Mathew are with the Department of Electrical Engineering, Government Engineering College, Thrissur 680009, India (e-mail: antonykannanaykal@gmail.com; jaison@ieee.org).

K. Gopakumar is with the Department of Electronics Systems Engineering, Indian Institute of Science, Bangalore 560012, India (e-mail: kgopa@iisc.ac.in).

Color versions of one or more figures in this article are available at https://doi.org/10.1109/TPEL.2022.3197362.

Digital Object Identifier 10.1109/TPEL.2022.3197362

and [25] are highly parameter dependent. Wu et al. [26] used a torque prediction controller together with a flexible duty ratio controller. Though the performance is improved, the simplicity of the DTC scheme is lost due to the estimation of near voltage vectors, sector identification, assessing the switching pattern, and duty ratio calculations. Wu et al. [27] and Abdelwahed et al. [28] proposed drive schemes that regulate the duty ratio of the applied voltage vector to minimize the voltage error and large variations in torque, respectively. In Abdelwahed et al. [28], steady-state torque error is eliminated by generating a virtual torque reference from an exponential moving average filter. However, the generation of reference stator flux and duty ratio calculation makes the controllers in [27] and [28] parameter-dependent and complex to implement. Furthermore, the error voltage between the reference voltage and the voltage vectors is higher in duty ratio control DTC and DSVM when compared to DTC-SVPWM. Consequently, DTC-SVPWM shows much better steady-state performance [26].

The objective of this work is to simplify the conventional DTC-SVPWM scheme and to make it less parameter dependent (i.e., the control algorithm does not make use of many motor parameters for its operation) without affecting the steady state and dynamic performances. Here, the approximate stator flux-linkage space vector needed to generate the reference torque is calculated in a simple manner. Once the reference flux vector is obtained, the corresponding stator phase-voltage reference needed for SVPWM is determined in every sampling period and an easy to implement, carrier-based space vector pulsewidth modulation scheme (CSVPWM) [29], [30], [31] is used for the modulation. The proposed control scheme requires only a single PI controller, uses less number of motor parameters for computation, is devoid of any rotational coordinate transformations and operates at constant switching frequency.

The rest of this article is organized as follows. Section II discusses the basic machine modeling needed for the analysis. The proposed drive scheme is derived and its control is explained in Section III. Sections IV and V discuss the simulation and hardware results, respectively. Finally, Section VI concludes this article.

II. Basic Theoretical Formulation

Electromagnetic torque of an induction motor controlled by DTC or DTC-SVPWM scheme [32] is given by

$$T = \frac{3}{2}\frac{P}{2}\frac{L_m}{\sigma L_s L_r}(|\psi_s||\psi_r|\ sin\ \theta_{sr}) \tag{1}$$

where the total leakage factor σ is given by

$$\sigma = 1 - \frac{L_m^2}{L_s L_r}. \tag{2}$$

Here, L_s, L_r, and L_m are stator self-inductance, rotor self-inductance, and the magnetizing inductance of the machine. $|\psi_s|$ and $|\psi_r|$ represent the magnitude of stator and rotor flux-linkage space vectors. θ_{sr} is the angle between stator and rotor flux-linkage space vectors and P indicates the number of poles in the machine.

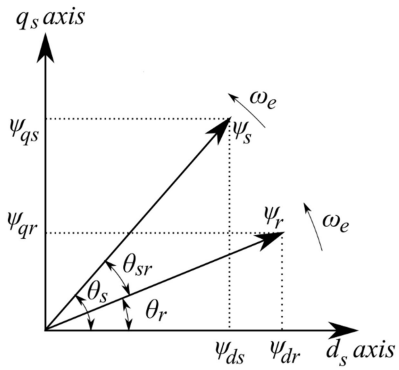

Fig. 1. Stator flux-linkage space vector and rotor flux-linkage space vector in the stationary reference frame.

During steady-state operation, stator and rotor flux-linkage space vectors ($\vec{\psi_s}$ and $\vec{\psi_r}$) rotate in uniform circular motion with constant angular frequency ω_e (see Fig. 1). According to (1), for low values of θ_{sr}, torque is proportional to θ_{sr} and θ_{sr} can be quickly regulated by controlling the stator flux-linkage space vector $\vec{\psi_s}$ by suitable selection of the stator voltage vectors. This is the basic principle behind the direct torque control scheme. From the induction motor's stator voltage equation, the magnitude and angle of the stator flux-linkage vectors can be written as shown in (3)–(6). The impact of stator resistance voltage drop is negligible at normal speed ranges [1], [33], [34] and hence it is not considered in this article. However, the stator resistance drop may also be included in the equations for low speed applications

$$\psi_{ds}(t) = \left(\int v_{ds}dt\right) + \psi_{ds}(t - \Delta t) \tag{3}$$

$$\psi_{qs}(t) = \left(\int v_{qs}dt\right) + \psi_{qs}(t - \Delta t) \tag{4}$$

$$|\psi_s| = \sqrt{\psi_{ds}^2 + \psi_{qs}^2} \tag{5}$$

$$\theta_s = \tan^{-1}\left(\frac{\psi_{qs}}{\psi_{ds}}\right) \tag{6}$$

where Δt denotes the sampling time. ψ_{ds} and ψ_{qs} are the direct and quadrature axis components of the stator flux-linkage space vector of the machine in the stationary reference frame. θ_s is the phase angle of the stator flux-linkage space vector $\vec{\psi_s}$. The rotor flux-linkage of the machine is given by

$$\psi_{dr} = (\psi_{ds} - \sigma L_s i_{ds})\frac{L_r}{L_m} \tag{7}$$

$$\psi_{qr} = (\psi_{qs} - \sigma L_s i_{qs})\frac{L_r}{L_m} \tag{8}$$

$$|\psi_r| = \sqrt{\psi_{dr}^2 + \psi_{qr}^2} \tag{9}$$

$$\theta_r = \tan^{-1}\left(\frac{\psi_{qr}}{\psi_{dr}}\right) \tag{10}$$

where ψ_{dr} and ψ_{qr} are the direct and quadrature axis components of the rotor flux-linkage space vector of the machine in

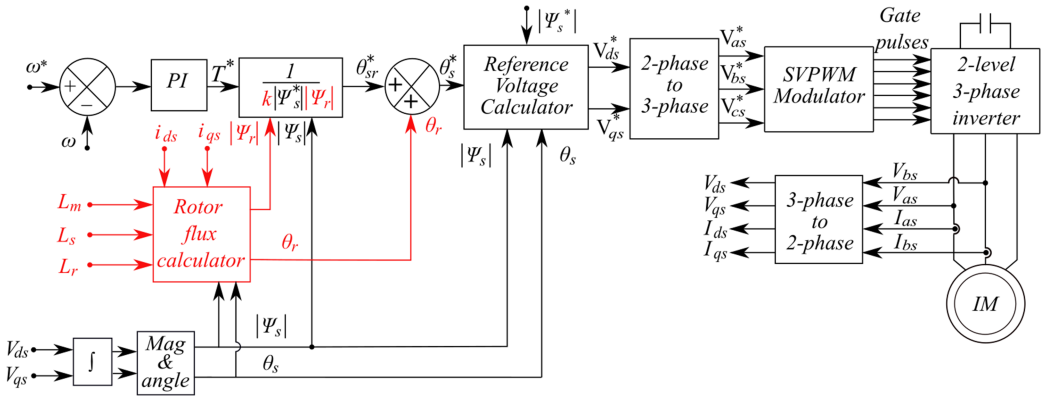

Fig. 2. General control scheme of DTC-SVPWM drive [13].

the stationary reference frame. θ_r gives the angle of the rotor flux-linkage vector $\vec{\psi}_r$.

A new control scheme is derived based on the above machine model equations as explained in the next section.

III. Development of the Proposed DTC-SVPWM Control Scheme

The proposed DTC speed control scheme is motivated by the drive scheme in [13], which has the desirable feature of using a single PI controller. However, the major issues in [13] are that the scheme depends on many rotor parameters and accurate computation of rotor flux linkage space vector is needed. In this work, the scheme is modified to make the drive completely free from rotor parameters and rotor flux linkage computation is unnecessary.

The general control strategy of DTC-SVPWM scheme in [13] is shown in Fig. 2. In the figure, the error between the reference and actual speed is used to determine the reference torque T^*. Based on (1), the reference torque angle between stator and rotor flux-linkage space vectors can be written as follows

$$\theta_{sr}^* = \sin^{-1}\left(\frac{T^*}{\frac{3}{2}\frac{P}{2}\frac{L_m}{\sigma L_s L_r}|\psi_s||\psi_r|}\right). \tag{11}$$

Addition of θ_{sr}^* and θ_r (rotor flux-linkage space vector angle) gives the reference angle of the stator flux-linkage θ_s^* (refer Fig. 1)

$$\theta_s^* = \theta_{sr}^* + \theta_r \tag{12}$$

where θ_r is computed using (7)–(10).

Applying suitable voltage vectors of the inverter for appropriate time intervals, the magnitude and angle of the stator flux-linkage vector can be controlled (see Fig. 3). That is, to generate the reference stator flux-linkage space vector $\vec{\psi}_s^*$, the controller needs to determine the instantaneous reference voltage that has to be applied during each sampling period Δt. Equations (3) and (4) can be used to compute the reference voltages (V_{ds}^* and V_{qs}^*) in the stationary reference frame as follows:

$$V_{ds}^* = \frac{\psi_{ds}^* - \psi_{ds}}{\Delta t} \tag{13}$$

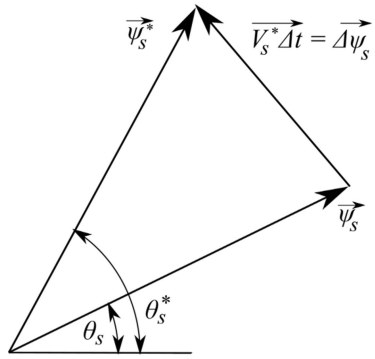

Fig. 3. Stator flux-linkage generation from reference voltage.

$$V_{qs}^* = \frac{\psi_{qs}^* - \psi_{qs}}{\Delta t} \tag{14}$$

where

$$\psi_{ds}^* = |\psi_s^*|\, cos\, \theta_s^* \tag{15}$$

$$\psi_{qs}^* = |\psi_s^*|\, sin\, \theta_s^* \tag{16}$$

$$\psi_{ds} = |\psi_s|\, cos\, \theta_s \tag{17}$$

$$\psi_{qs} = |\psi_s|\, sin\, \theta_s. \tag{18}$$

The controller calculates $|\psi_s|$ and θ_s using (5) and (6). The magnitude of the reference stator flux-linkage vector $|\psi_s^*|$ is held constant at its rated value below base speed of the motor.

The d-q reference voltages are then converted to three-phase reference voltages for realizing space vector pulse width modulation (SVPWM) using two-phase to three-phase transformation.

The main advantage of the scheme is that it uses a single PI controller to generate the reference stator flux-linkage vector $\vec{\psi}_s^*$. However, the control scheme depends on several motor parameters (see Fig. 2). To make the controller less dependent on rotor parameters, and to further simplify the scheme, a few simplifying assumptions are made as follows:

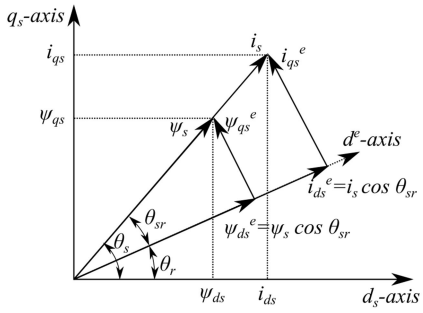

Fig. 4. Relationship between current and flux linkages in stationary reference frame and reference frame aligned to rotor flux.

A. Rotor Flux-Linkage Vector is Stationary During Any Particular Sampling Period

The sampling frequency of the controller is taken much higher than the fundamental frequency. Therefore, compared to stator flux-linkage space vector, the rotor flux-linkage space vector can be assumed to be stationary during any sampling period as the time constant of the rotor circuit is much greater than the stator circuit (see Fig. 1)

$$\theta_s^* = \theta_{sr}^* - \theta_{sr} + \theta_s \quad [= (\theta_s^* - \theta_r) - (\theta_s - \theta_r) + \theta_s]. \tag{19}$$

B. Rotor and Stator Flux-Linkage Magnitudes are Approximately Equal

Based on the induction motor dynamic model in the reference frame aligned to the rotor flux, the expressions for d^e-axis (direct excitation axis) rotor voltage v_{dr}^e, and d^e-axis stator and rotor flux linkage space vectors (ψ_{ds}^e & ψ_{dr}^e) are given by [35]

$$v_{dr}^e = i_{dr}^e R_r + \frac{d}{dt}(\psi_{dr}^e) \tag{20}$$

$$\psi_{dr}^e = |\psi_r| = L_r i_{dr}^e + L_m i_{ds}^e \tag{21}$$

$$\psi_{ds}^e = L_s i_{ds}^e + L_m i_{dr}^e \tag{22}$$

where i_{ds}^e is the d^e-axis stator current and R_r is the rotor resistance. During steady-state operation, $|\psi_{dr}^e|$ is held constant. Hence, $\frac{d}{dt}(\psi_{dr}^e)$ is zero. Substituting this into (20) gives

$$i_{dr}^e = 0. \tag{23}$$

Plugging (23) into (21) and (22) gives

$$\psi_{dr}^e = |\psi_r| = L_m i_{ds}^e \tag{24}$$

$$\psi_{ds}^e = L_s i_{ds}^e. \tag{25}$$

From Fig. 4, ψ_{ds}^e and i_{ds}^e can be written in terms of θ_{sr} as shown below:

$$i_{ds}^e = i_s cos\,\theta_{sr}. \tag{26}$$

$$\psi_{ds}^e = \psi_s cos\,\theta_{sr} \tag{27}$$

Substituting (26)–(27) into (24)–(25) gives the relationship between the stator and rotor flux linkages as given in the following:

$$\psi_r = \psi_s \frac{L_m}{L_s} cos\,\theta_{sr}. \tag{28}$$

Typical values of $\frac{L_m}{L_s}$ and $cos\,\theta_{sr}$ are in the range of 0.97 to 0.99 and 0.98 to 0.99, respectively [35], [36] and hence, the magnitude of stator and rotor flux-linkages can be assumed to be constant and equal in any particular switching time period ($|\psi_s| \approx |\psi_r|$).

Since θ_{sr} is very small, sin(θ_{sr}) is approximated to θ_{sr}. Therefore, (1) and (11) can be simplified and used to determine θ_{sr} and θ_{sr}^* as given below:

$$\theta_{sr} = \frac{T}{k|\psi_s^2|} \tag{29}$$

$$\theta_{sr}^* = \left(\frac{T^*}{k|\psi_s^*|^2}\right) \tag{30}$$

where

$$k = \frac{3}{2}\frac{P}{2}\frac{L_m}{\sigma L_s L_r}. \tag{31}$$

C. Proposed Drive Scheme

To compute θ_{sr}, the instantaneous machine torque T needs to be determined, which can be calculated as follows:

$$T = \frac{3}{2}\frac{P}{2}(i_{qs}\psi_{ds} - i_{ds}\psi_{qs}) \tag{32}$$

where i_{ds} and i_{qs} are the direct and quadrature axis components of stator currents in the stationary reference frames. Solving (19) by plugging in θ_{sr} and θ_{sr}^* from (29)–(30) gives

$$\theta_s^* = \frac{1}{k}\left(\frac{T^*}{|\psi_s^*|^2} - \frac{T}{|\psi_s|^2}\right) + \theta_s. \tag{33}$$

The value of k given in (31) depends on the rotor flux-linkage, magnetizing and leakage inductances of stator and rotor windings. In this control scheme, the value of k is estimated approximately without using any motor parameters. For a typical value of θ_{sr}, and for the rated stator flux-linkage and torque, the value of "k" can be determined using (29). If the value of k estimated using (29) is greater than the actual value, θ_s^* becomes less than needed [refer (33)], which decreases θ_{sr} and machine torque [refer (1)]. Reduction in machine torque increase the speed error and necessitates a rise in PI controller output (reference torque T^*). The increase in T^* finally increases θ_s^* and vice versa. Therefore, any error in the estimation of k value due to the aforementioned simplifying assumptions are nullified by the PI controller.

Based on the above discussion, the control strategy is modified as shown in Fig. 5. The proposed control scheme avoids the use of rotor parameters for its implementation and operates with a single PI controller. The parameters and blocks shown in red color in Fig. 2 are not used in this control, which makes the parameter dependence of the proposed drive similar to that of the conventional DTC scheme. Moreover, the proposed control logic uses carrier-based space vector modulation technique

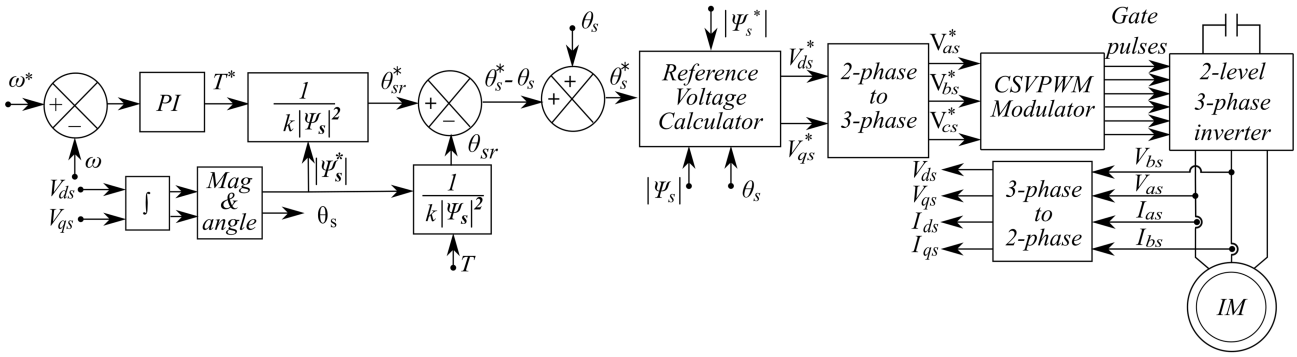

Fig. 5. Control strategy of the proposed drive.

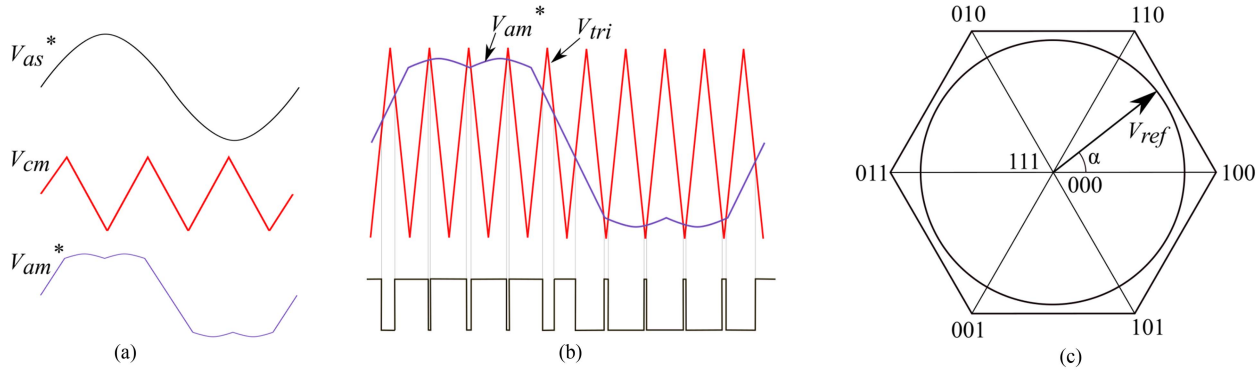

Fig. 6. Gate pulse generation using CSVPWM technique. (a) Generation of modulating signal V^*_{am}. (b) Generation of PWM gate signals of phase-A. (c) Space vector diagram

(CSVPWM) instead of conventional space vector modulation as follows:

The direct axis and quadrature axis components of reference voltage in the stationary reference frame V^*_{ds} and V^*_{qs} are calculated using (13)–(14). Now, two-phase to three-phase transformation is carried out to get three-phase reference voltages (V^*_{as}, V^*_{bs} and V^*_{cs})

$$V^*_{as} = V^*_{ds} \tag{34}$$

$$V^*_{bs} = \frac{-V^*_{ds} + \sqrt{3}V^*_{qs}}{2} \tag{35}$$

$$V^*_{cs} = \frac{-V^*_{ds} - \sqrt{3}V^*_{qs}}{2}. \tag{36}$$

For example, assume the rated stator flux-linkage of the machine is $|\psi^*_s| = 1$ Vs, actual stator flux-linkage magnitude $|\psi_s| = 0.95$ Vs, DC rail voltage, $V_{dc} = 600$ V, $\theta_s = 28°$, $\theta^*_s = 30°$, and sampling time $\Delta t = 0.25$ ms. By using (13)–(14), the reference value of voltage vectors in the direct and quadrature axis in stationary reference frame is found to be $V^*_{ds} = 109$ V and $V^*_{qs} = 216$ V. Inverse Clarke's transformation as shown in (35)–(37) can be used to determine the three-phase reference voltages V^*_{as} =109 V, $V^*_{bs} = 133$ V, and $V^*_{cs} = -242$ V.

These three-phase reference voltages are utilized to generate CSVPWM pulses as follows. A triple-n harmonic signal Vcm (common mode voltage) is added to the reference voltage to generate the modulating signals for CSVPWM [29], [37]. The modulating signal and common mode voltage are shown in Fig. 6(a). Equations (37)–(39) are used for the generation of V_{cm} from the three-phase reference voltages

$$V_{cm} = \frac{-(V_{max} + V_{min})}{2} \tag{37}$$

where

$$V_{max} = max(V^*_{as}, V^*_{bs}, V^*_{cs}) \tag{38}$$

$$V_{min} = min(V^*_{as}, V^*_{bs}, V^*_{cs}). \tag{39}$$

The modulating signals of each phase is given by

$$V^*_{xm} = V_{xs} + V_{cm}, \quad where\ x = a\ or\ b\ or\ c. \tag{40}$$

Modulating signals of each phase, after suitable scaling to the carrier level, are then compared with a high-frequency triangular carrier wave [see Fig. 6(b)]. The space vector and the locus of the resultant voltage space vector during steady state are shown in Fig. 6(c).

Compared to conventional space vector modulation technique, there is no need for sector identification and trigonometric mathematical computations to generate the switching pulses.

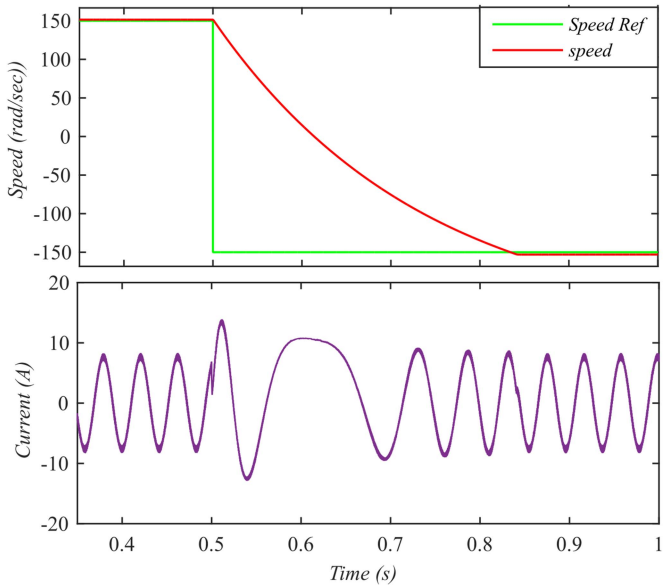

Fig. 7. Phase current waveform of the proposed drive during speed reversal from 150 rd/s to −150 rd/s at no-load for a switching frequency of 4 kHz.

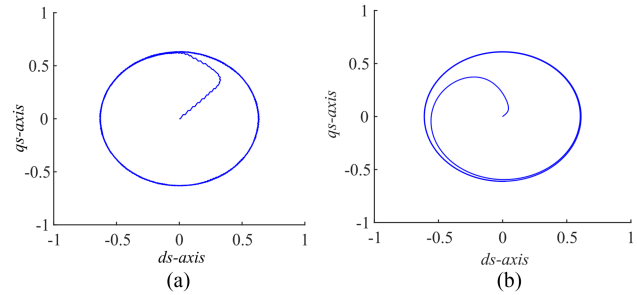

Fig. 8. Stator flux-linkage and rotor flux-linkage trajectories in the stationary reference frame at no load. (a) Stator flux-linkage. (b) Rotor flux-linkage.

IV. Simulation Results

The performance of the proposed scheme is verified using MATLAB simulations, which is carried out at a switching frequency of 4 kHz. Fig. 7 shows the speed and current transients of the proposed drive when a speed reversal command is executed at 0.5 s. It can be seen that the speed is reversed smoothly from 150 rd/s to −150 rd/s at no load in 320 ms without any appreciable transients in stator current. Fig. 8(a) and (b) shows the trajectory of the stator and rotor flux-linkage vectors of the proposed drive. Both stator and rotor flux-linkage vectors have uniform circular trajectory without noticeable ripples.Figs. 9 and 10 show the three-phase stator current waveforms of classical DTC and DTC-SVPWM [13] schemes respectively, for an average switching frequency of 4 kHz. The stator current total harmonic distortion (THD) of traditional DTC scheme is 24.2% and for the scheme in [13] it is found to be 5.1%. Fig. 11 shows the three-phase stator current waveform of the proposed drive. The current THD of the proposed scheme is found to be the same as that of drive scheme in [13]. Fig. 12 shows the torque waveform of the classical DTC scheme, which has a peak ripple magnitude of 40% of the load torque for an average switching

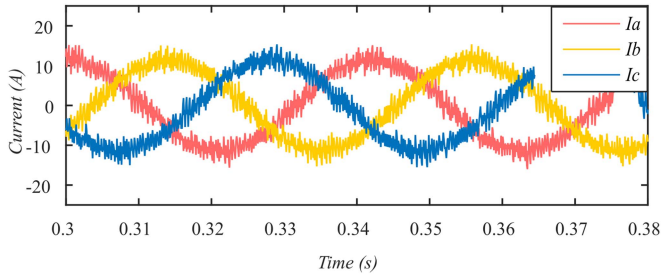

Fig. 9. Three-phase stator current waveforms of the conventional DTC drive for a load torque of 10 Nm and average switching frequency of 4 kHz.

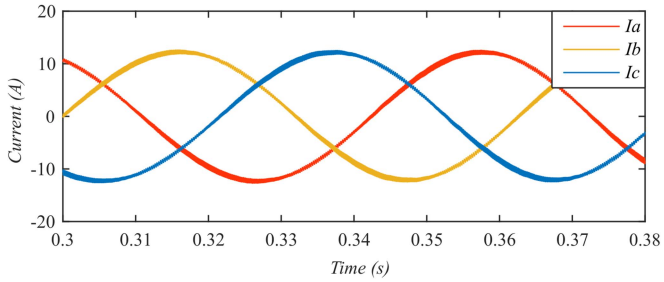

Fig. 10. Three-phase stator current waveforms of the scheme in [13] drive for a load torque of 10 Nm and switching frequency of 4 kHz.

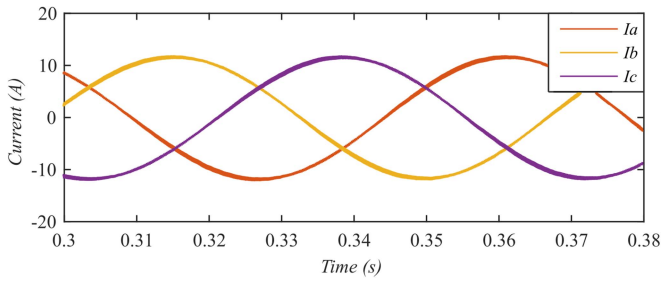

Fig. 11. Three-phase stator current waveforms of proposed drive for a load torque of 10 N_m and switching frequency of 4 kHz.

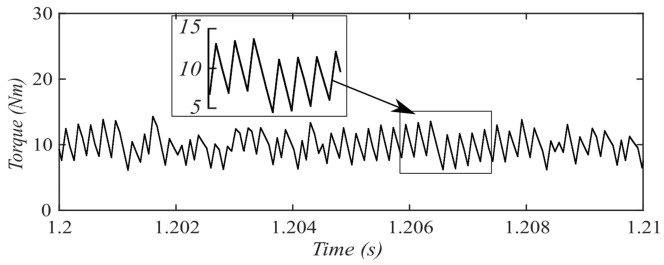

Fig. 12. Torque versus time (Classical DTC scheme).

frequency of 4 kHz. The torque ripple of the scheme in [13] and that of the proposed drive are shown in Figs. 13 and 14, respectively. The peak torque ripple magnitude is found to be 8% of the load torque in both the schemes.

The FFT analysis of stator currents for three schemes (classical DTC, drive scheme in [13] and proposed drive) and for different load torques are depicted in Fig. 15. Their peak torque ripple magnitudes for different loads and switching frequencies are plotted in Figs. 16 and 17. Varying the load has no significant

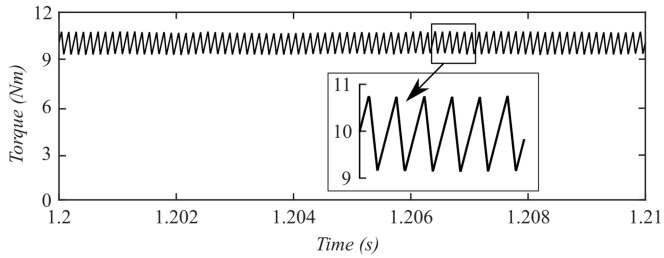

Fig. 13. Torque versus time (DTC-SVPWM scheme in [13]).

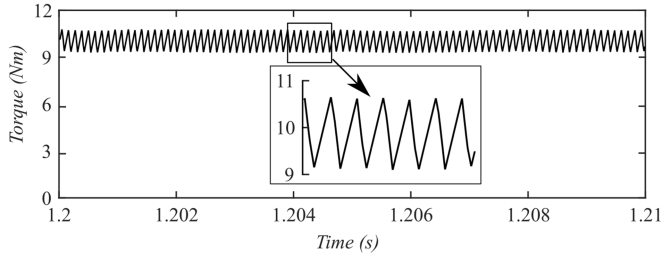

Fig. 14. Torque versus time (Proposed drive).

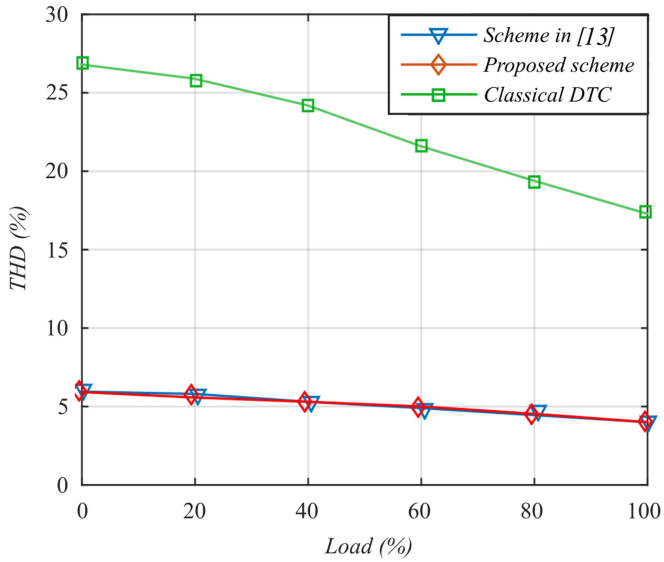

Fig. 15. THD versus load ((Blue line: Scheme in [13], Red line: Proposed drive, Green line: Classical DTC).

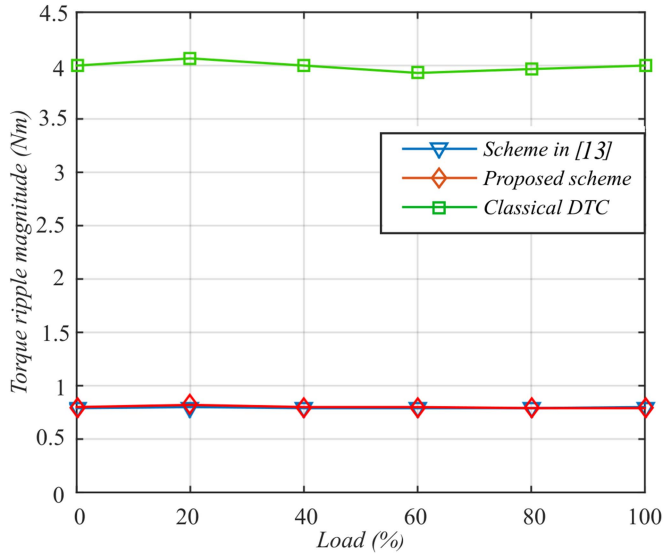

Fig. 16. Torque ripple versus Load (Blue line: Scheme in [13], Red line: Proposed drive, Green line: Classical DTC).

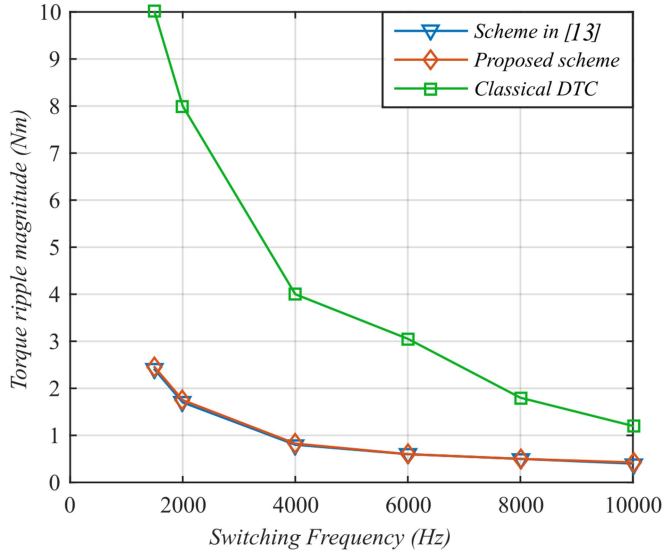

Fig. 17. Torque ripple versus switching frequency (Blue line: Scheme in [13], Red line: Proposed drive, Green line: Classical DTC).

effect on the torque ripple. However, increasing the switching frequency reduces the torque ripple. Figs. 15–17 shows that the proposed drive and drive DTC-SVPWM (scheme in [13]) have similar characteristics in terms of torque ripple and current THD.

V. Hardware Results

A 2 HP, 415 V, 50 Hz, 4 Pole, 1420 RPM three-phase induction motor is used to realize the hardware with the help of a TMS320F28335 DSP processor. The inverter, microcontroller unit (MCU), and motor specifications are given in Table I. The inverter is operated at a switching frequency of 4 kHz. Motor speed is sensed using a 10-bit encoder. LA-55P and LV-20P

TABLE I
Inverter, MCU, and Motor Specifications

Components	Specifications
Motor specification	Three-Phase induction motor Power: 2HP Voltage: 415V Current: 3.4A Speed: 1420 r/min Poles: 4
Incremental encoder	ENC58-S10 Pulse per rotation: 1024ppr
Converter specification	IGBT: SKM100GB12T4 DC rail Capacitor: 1100μF
DSP Processor	TMS320f28335 Clock Frequency:150MHz

TABLE II
PROGRAM EXECUTION TIME FOR DIFFERENT SCHEMES

DTC	$20\mu s$
DTC-SVPWM (scheme in [13])	$33\mu s$
Proposed scheme	$24\mu s$

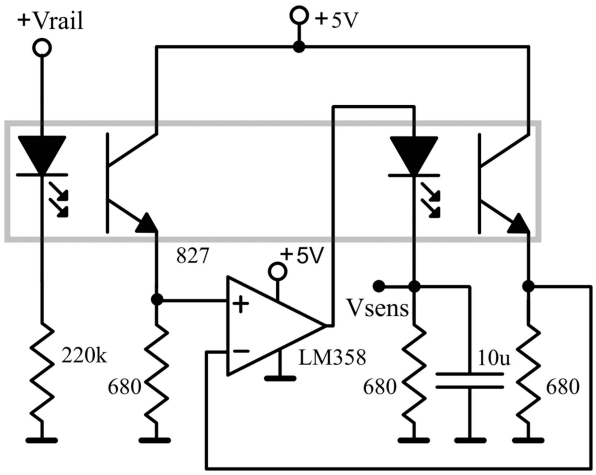

Fig. 18. Low-cost optocoupler based voltage sensor.

sensors are used to sense the current and voltage, respectively. A second-order Butterworth low-pass filter based on a high slew rate Op-Amp MC34074 filters the feedback voltage and current. To calculate the phase voltages of the machine, only dc link voltage is sensed. The method of calculating phase voltages from dc link voltages is given in [38].

Instead of expensive hall effect-based voltage transducers to provide galvanic isolation, voltage sensors based on linear optocouplers may also be used [39]. As the proposed scheme computes pole voltages using the dc rail voltage measurement, the bandwidth requirement of the voltage sensor is less stringent and hence, an extremely low-cost dual optocoupler based voltage sensor as presented in Fig. 18 may be used in low-cost applications. One issue with optocoupler based voltage sensors is the drift in the current transfer ratio (CTR) with temperature, which is nullified by negative feedback. The operational amplifier in the circuit will try to keep the voltages at its input terminals equal and any increase in voltage due to CTR drift at the output of the first optocoupler gets nullified due to a corresponding reduction in the light emitting diode current of the second optocoupler so that the measured voltage (V_{sens}) is precise and less affected by CTR changes. The experiments when repeated with this low-cost alternative yield similar results. A photograph of the experimental setup is shown in Fig. 19.

The speed reversal characteristics of the motor when the speed changes from +1000 r/min to −1000 r/min is shown in Fig. 20. The motor speed is estimated by the DSP processor using encoder pulses and is outputted by the digital to the analog module of the controller. The speed reversal command is given at instant "A" using a rate limiter having a slope of 800 rpm/s. The speed reversal operation completes at instant B. The speed reversal occurs smoothly without any significant transient overshoot or undershoot in current.

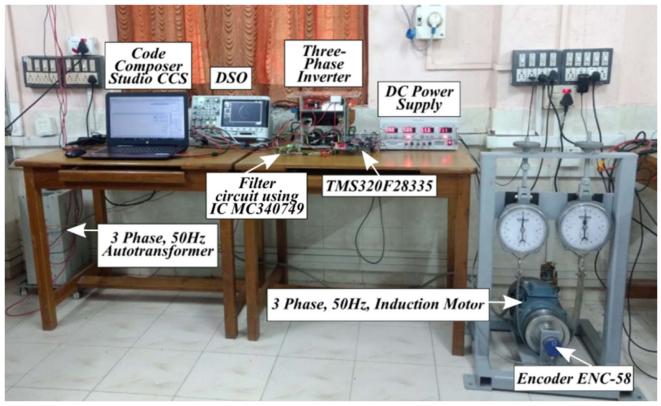

Fig. 19. Experimental setup.

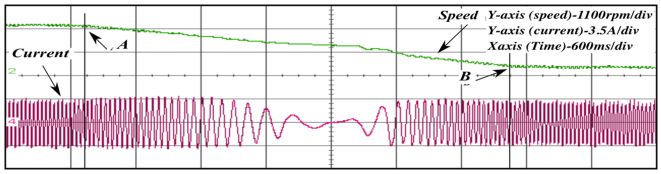

Fig. 20. Speed reversal characteristics with a rate limiter of slope 800 rpm/s is used to give the speed command (First Trace: Motor speed, Second Trace: Stator current of Phase-A).

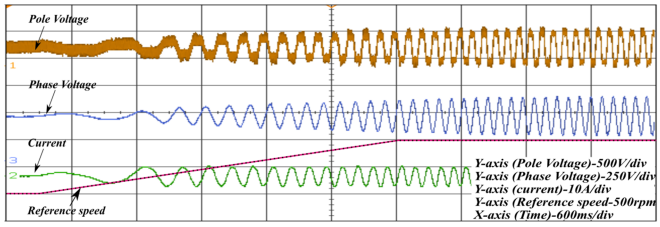

Fig. 21. Motor starting characteristics with a rate limiter of slope 300 rpm/s is used to give the speed command (First Trace: Pole voltage of Phase-A, Second Trace: Phase-A phase voltage, Third Trace: Stator current of phase-A, Fourth Trace: Reference speed).

The pole voltage, phase voltage, and the stator current of the machine during the starting transient with and without a rate limiter for speed command are shown in Figs. 21 and 22, respectively. Fig. 21 demonstrates the smooth and slow acceleration of the machine during starting from rest to 750 r/min. In Fig. 22, the motor response is made quicker by removing the rate limiter for speed command. The pole voltage, phase voltage, and current reaches its steady state in less than 100 ms, which shows the fast response of the proposed drive scheme to the speed command. The peak overshoot in current is less than 2.5 times the rated current of the motor. The pole voltages are measured using high voltage differential voltage probes (Tektronics P5200 A) and the phase voltage is computed [38] and outputted using the digital to analog port of the controller. The stator currents are measured using current probes (Tektronics A621).

The stator current of traditional DTC scheme for an average switching frequency of 4 kHz is shown in Fig. 23(a). The average switching frequency is calculated using the DSP processor by counting the number of switch transitions in each second. It can be observed that the current ripple is quite high (45.67% THD)

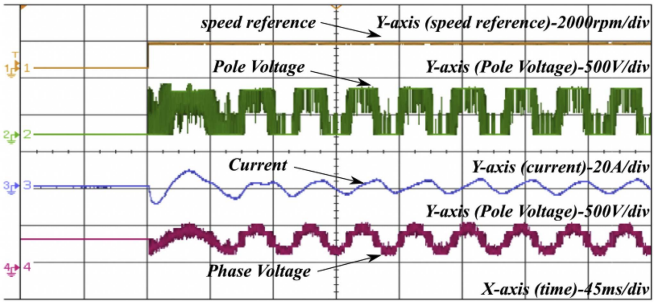

Fig. 22. Motor starting characteristics without using a rate limiter to give the speed command (First Trace: Reference speed, Second Trace: Pole voltage of Phase-A, Third Trace: Stator current of phase-A, Fourth Trace: Phase-A phase voltage).

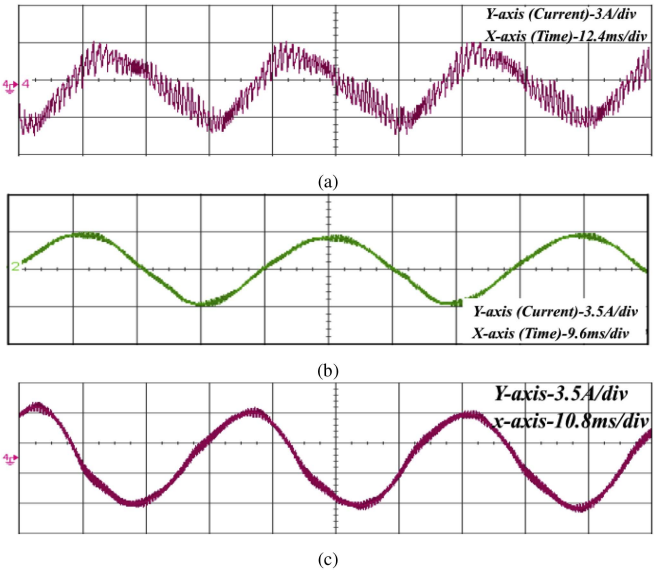

Fig. 23. Stator current of phase-A for (a) conventional DTC, (b) DTC-SVPWM [13] and (c) proposed drive.

even at an average switching frequency of 4 kHz. To achieve this switching frequency, the sampling rate of the processor needed is 40 kHz. Higher switching frequency corresponds to faster control action which calls for higher sampling rate; and a low program execution time will help to achieve this. The stator current waveforms of the DTC-SVPWM [13] and the proposed drive in this article for a switching frequency of 4 kHz are shown in Figs. 23(b) and (c), respectively. The THD of the stator current of the proposed drive is found to be 7.31% which is almost the same as that of the DTC-SVPWM scheme (7.35%). The THD of all the schemes are determined by taking the experimental data points and analyzing it using MATLAB software. The steady-state percentage torque ripple magnitude of the conventional DTC scheme is 50.2% [see Fig. 24(a)]. For the DTC-SVPWM (scheme in [13]) and for the proposed drive scheme, the percentage torque ripple magnitude at steady state is found to be almost the same at 12.4% and 12.2% [Fig. 24(b) and (c)], respectively.

Equation (33) is derived based on the assumption that the angle between stator and rotor flux linkage space vector θ_{sr} is very small as mentioned in Section III-C. However, the small

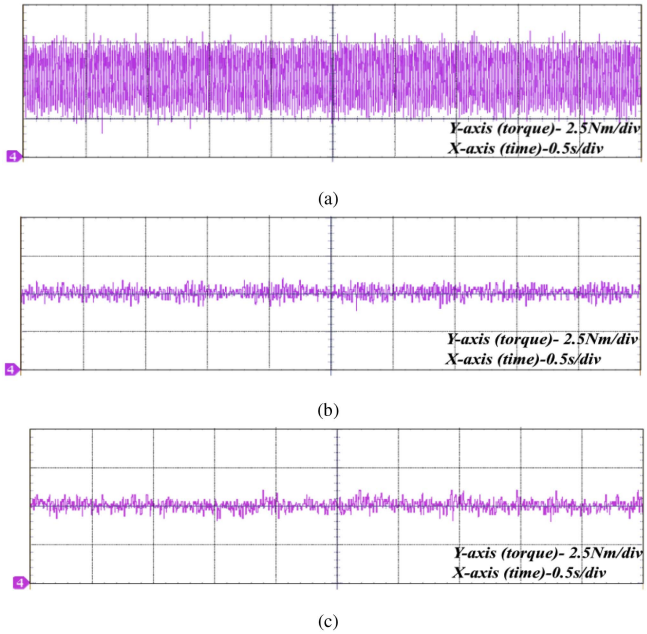

Fig. 24. Steady-state torque ripple for a load of 5 N · m (a) conventional DTC, (b) DTC-SVPWM [13], and (c) proposed drive.

angle approximation is valid upto about 20° and to get a fast torque response θ_{sr}^{*} should be as high as maximum during transients, approaching 90°. However, this can affect the torque ripple during transients. Thus, there is a tradeoff between fast response and torque ripple during transients. When the machine approaches steady-state operation, θ_{sr}^{*} comes down to a small value due to the action of PI controller.

Fig. 25 shows the torque and speed tracking for the conventional DTC, DTC-SVPWM [13] and the proposed drive. Initially, the speed command is changed from 0 to 750 r/min and then to -750 r/min afterward with a load torque of 5Nm. To show the quick torque and speed response, these waveforms are taken without any rate limiter. For conventional DTC scheme, machine starting time is 66 ms and the speed reversal time is 122 ms. The proposed scheme accelerates the machine in 77 ms and completes the speed reversal in 128 ms. In DTC-SVPWM, the machine takes 80 ms to accelerate and 130 ms for speed reversal.

Stator flux-linkage of the machine for a speed of 1000 r/min is shown in Fig. 26, which is computed based on (3) and (4). Fig. 26(a) shows the stator flux-linkage waveform and the corresponding circular trajectory is given in Fig. 26(b). It can be noted that the stator flux follows a near-circular trajectory with low distortion. To show the flux estimation accuracy at low speeds, the stator flux trajectory, the speed and the current waveforms for different low frequency operations (1 Hz, 1.75 Hz and 5 Hz) are shown in Fig. 27. Satisfactory performance is obtained even at a very low speed of 1 Hz. The flux vector maintains the circular locus with the flux vector magnitude almost constant without much ripple. When the frequency increases to above 5 Hz, the current and flux vector trajectory have very good accuracy.

The program execution time is 20μs for the conventional DTC whereas the program execution time taken by DTC-SVPWM and proposed schemes are 33μs and 24μs, respectively (refer

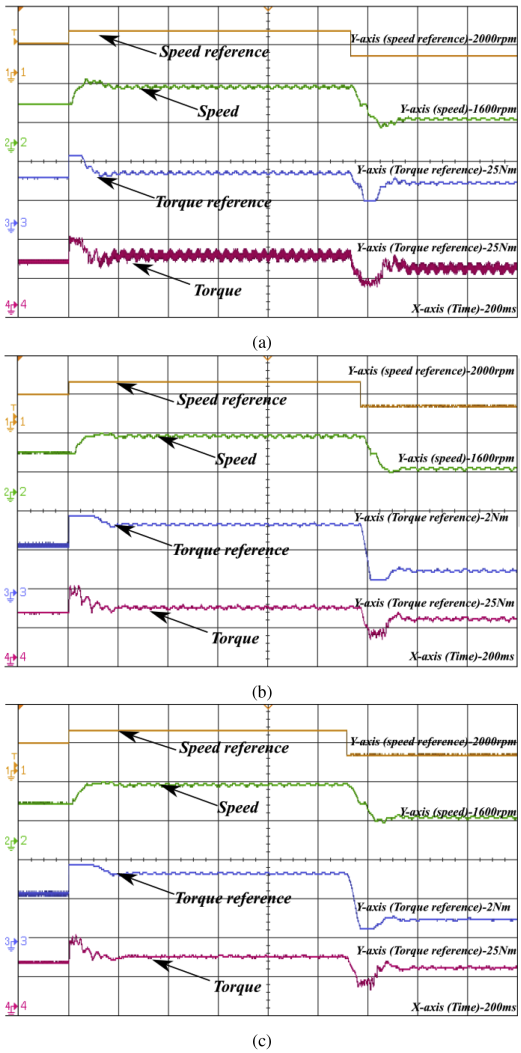

Fig. 25. Torque and speed tracking without using a speed rate limiter for a load torque of 5 N · m (a) conventional DTC, (b) DTC-SVPWM [13], and (c) proposed drive.

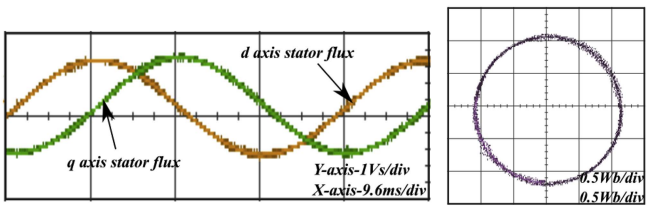

Fig. 26. Stator flux-linkage waveforms of proposed drive (33 Hz). (a) Stator flux-linkage in stationary reference frame (b) Stator flux-linkage space vector trajectory.

Table II). This indicates 27% lower computational time for the proposed method compared to DTC-SVPWM. Though, the execution time is slightly higher compared to the conventional DTC scheme, the current ripple performance and torque ripple performance (Figs. 23 and 24) are much inferior in the classical DTC scheme for the same average switching frequency. If the torque ripple performance of the classical DTC needs to be improved, a much higher sampling rate will be needed which

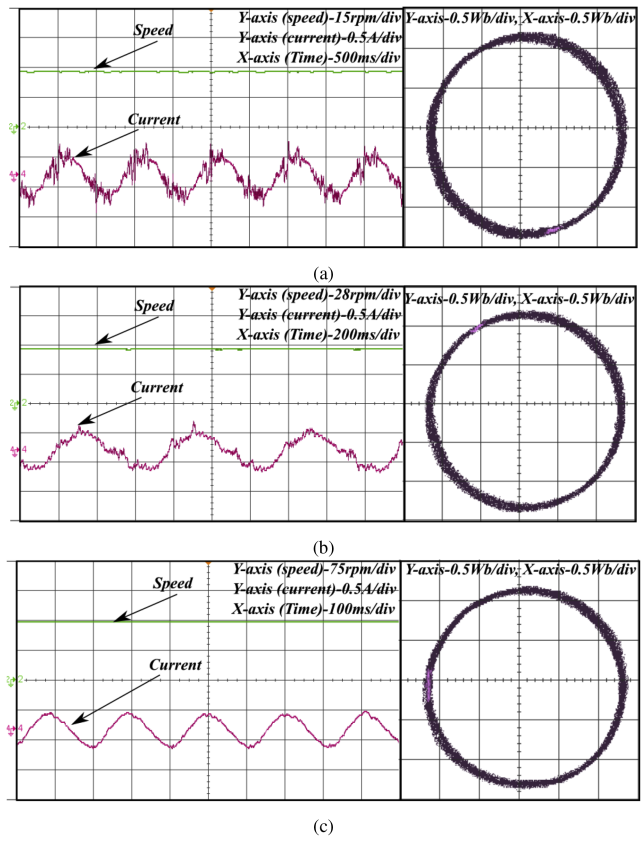

Fig. 27. Speed, current and stator flux trajectory for low speed operation (a) 1 Hz operation, (b) 1.75 Hz operation and (c) 5 Hz operation.

will necessitate high performance (high cost) MCU whereas for the proposed method, lower sampling rate is sufficient due to constant switching frequency SVPWM.

VI. Conclusion

A new control scheme for carrier-based space vector modulated DTC drive has been developed based on the machine model. The proposed drive scheme requires only a single PI controller, the control scheme is independent of rotor parameters, and no rotor flux computation is needed. More importantly, all mathematical computations are done in the stationary reference frame, which considerably reduce the computational efforts. A carrier-based space vector modulation is used for SVPWM which further simplify the calculations involved and gives very good steady-state performance. Simulation and hardware results on a 2 HP, 415 V three-phase induction motor drive have been presented to validate the effectiveness of the proposed drive scheme. Comparison between the proposed and conventional DTC-SVPWM drive show that the performance of both the proposed and conventional scheme are similar in terms of torque and current THD. However, the control scheme of the proposed drive is intuitive, much easier to implement, computational time is reduced by 27% and uses less number of motor parameters. A low cost optocoupler based voltage sensor is also presented to reduce the overall cost of the system.

REFERENCES

[1] I. Takahashi and T. Noguchi, "A new quick-response and high-efficiency control strategy of an induction motor," *IEEE Trans. Ind. Appl.*, vol. IA-22, no. 5, pp. 820–827, Sep. 1986.

[2] Y.-S. Lai and J.-H. Chen, "A new approach to direct torque control of induction motor drives for constant inverter switching frequency and torque ripple reduction," *IEEE Trans. Energy Convers.*, vol. 16, no. 3, pp. 220–227, Sep. 2001.

[3] J. N. Nash, "Direct torque control, induction motor vector control without an encoder," *IEEE Trans. Ind. Appl.*, vol. 33, no. 2, pp. 333–341, Mar./Apr. 1997.

[4] A. K. Peter and J. Mathew, "Rotor parameter independent carrier space vector modulated direct torque control of induction motor," in *Proc. IEEE Transp. Electrific. Conf.*, 2019, pp. 1–6.

[5] A. Bazzi, A. Friedl, S. Choi, and P. T. Krein, "Comparison of induction motor drives for electric vehicle applications: Dynamic performance and parameter sensitivity analyses," in *Proc. IEEE Int. Electric Machines Drives Conf.*, 2009, pp. 639–646.

[6] S. N. Pandya and J. Chatterjee, "Torque ripple minimization in DTC based induction motor drive using carrier space vector modulation technique," in *Proc. Joint Int. Conf. Power Electron., Drives Energy Syst. Power India*, 2010, pp. 1–7.

[7] U. Senthil and B. Fernandes, "Hybrid space vector pulse width modulation based direct torque controlled induction motor drive," in *Proc. IEEE 34th Annu. Conf. Power Electron. Specialist*, 2003, pp. 1112–1117.

[8] A. Tripathi, A. M. Khambadkone, and S. K. Panda, "Torque ripple analysis and dynamic performance of a space vector modulation based control method for AC-drives," *IEEE Trans. Power Electron.*, vol. 20, no. 2, pp. 485–492, Mar. 2005.

[9] A. Kumar, B. Fernandes, and K. Chatterjee, "Simplified svpwm-dtc of 3-phase induction motor using the concept of imaginary switching times," in *Proc. 30th Annu. Conf. IEEE Ind. Electron. Soc.*, 2004, pp. 341–346.

[10] G. Satheesh, T. B. Reddy, and C. S. Babu, "Four level decoupled SVPWM based direct torque control (DTC) of open end induction motor drive," in *Proc. Int. Conf. Adv. Power Convers. Energy Technol.*, 2012, pp. 1–5.

[11] D. Casadei, G. Serra, A. Tani, L. Zarri, and F. Profumo, "Performance analysis of a speed-sensorless induction motor drive based on a constant-switching-frequency DTC scheme," *IEEE Trans. Ind. Appl.*, vol. 39, no. 2, pp. 476–484, Mar./Apr. 2003.

[12] C. Lascu, S. Jafarzadeh, M. S. Fadali, and F. Blaabjerg, "Direct torque control with feedback linearization for induction motor drives," *IEEE Trans. Power Electron.*, vol. 32, no. 3, pp. 2072–2080, Mar. 2017.

[13] J. Rodriguez, J. Pontt, C. Silva, S. Kouro, and H. Miranda, "A novel direct torque control scheme for induction machines with space vector modulation," in *Proc. IEEE 35th Annu. Power Electron. Specialists Conf.*, 2004, pp. 1392–1397.

[14] A. Peter and J. Mathew, "Bus clamped space vector pulse width modulated direct torque control of induction motor," in *Proc. IEEE Region 10 Symp.*, 2019, pp. 508–513.

[15] G. S. Buja and M. P. Kazmierkowski, "Direct torque control of PWM inverter-fed AC motors–A survey," *IEEE Trans. Ind. Electron.*, vol. 51, no. 4, pp. 744–757, Aug. 2004.

[16] S. K. De, P. Baishya, and S. Chatterjee, "Speed sensor-less rotor flux oriented control of a 3-phase induction motor drive using SVPWM," in *Proc. Int. Conf. Intell. Comput. Control Syst.*, 2019, pp. 612–616.

[17] A. Pal, S. Das, and A. K. Chattopadhyay, "An improved rotor flux space vector based MRAS for field-oriented control of induction motor drives," *IEEE Trans. Power Electron.*, vol. 33, no. 6, pp. 5131–5141, Jun. 2018.

[18] U. Syamkumar and B. Jayanand, "Real-time implementation of sensorless indirect field-oriented control of three-phase induction motor using a kalman smoothing-based observer," *Int. Trans. Elect. Energy Syst.*, vol. 30, no. 2, 2020, Art. no. e12242.

[19] K. Wang, Y. Li, Q. Ge, and L. Shi, "An improved indirect field-oriented control scheme for linear induction motor traction drives," *IEEE Trans. Ind. Electron.*, vol. 65, no. 12, pp. 9928–9937, Dec. 2018.

[20] D. L. Mon-Nzongo, T. Jin, G. Ekemb, and L. Bitjoka, "Decoupling network of field-oriented control in variable-frequency drives," *IEEE Trans. Ind. Electron.*, vol. 64, no. 7, pp. 5746–5750, Jul. 2017.

[21] Z. Guo, J. Zhang, Z. Sun, and C. Zheng, "Indirect field oriented control of three-phase induction motor based on current-source inverter," *Procedia Eng.*, vol. 174, pp. 588–594, 2017.

[22] S. Yang, D. Ding, X. Li, Z. Xie, X. Zhang, and L. Chang, "A novel online parameter estimation method for indirect field oriented induction motor drives," *IEEE Trans. Energy Convers.*, vol. 32, no. 4, pp. 1562–1573, Dec. 2017.

[23] K. Wang, R. D. Lorenz, and N. A. Baloch, "Enhanced methodology for injection-based real-time parameter estimation to improve back EMF self-sensing in induction machine deadbeat-direct torque and flux control drives," *IEEE Trans. Ind. Appl.*, vol. 54, no. 6, pp. 6071–6080, Nov./Dec. 2018.

[24] M. Amiri, J. Milimonfared, and D. A. Khaburi, "Predictive torque control implementation for induction motors based on discrete space vector modulation," *IEEE Trans. Ind. Electron.*, vol. 65, no. 9, pp. 6881–6889, Sep. 2018.

[25] I. Osman, D. Xiao, M. F. Rahman, M. Norambuena, and J. Rodriguez, "Discrete space vector modulation based model predictive flux control with reduced switching frequency for IM drive," *IEEE Trans. Energy Convers.*, vol. 36, no. 2, pp. 1357–1367, Jun. 2021.

[26] X. Wu, W. Huang, Y. Zhao, and C. Huang, "An efficient model predictive torque control for induction motors with flexible duty ratio optimization," *IEEE J. Emerg. Sel. Topics Power Electron.*, vol. 10, no. 4, pp. 4014–4025, Aug. 2022.

[27] X. Wu, W. Huang, X. Lin, W. Jiang, Y. Zhao, and S. Zhu, "Direct torque control for induction motors based on minimum voltage vector error," *IEEE Trans. Ind. Electron.*, vol. 68, no. 5, pp. 3794–3804, May 2021.

[28] A. N. Abdelwahed, C. Gu, X. Wang, G. Buticchi, S. Bozhko, and C. Gerada, "Torque performance improvement for direct torque controlled PMSM drives based on duty ratio regulation," *IEEE Trans. Power Electron.*, vol. 37, no. 1, pp. 749–760, Jan. 2022.

[29] Y.-H. Lee, R.-Y. Kim, and D.-S. Hyun, "A novel SVPWM strategy considering DC-link balancing for a multi-level voltage source inverter," in *Proc. 14th Annu. Appl. Power Electron. Conf. Exp.*, 1999, pp. 509–514.

[30] F. Wang, "Sine-triangle versus space-vector modulation for three-level PWM voltage-source inverters," *IEEE Trans. Ind. Appl.*, vol. 38, no. 2, pp. 500–506, Mar./Apr. 2002.

[31] M. M. Gaballah, "Design and implementation of space vector PWM inverter based on a low cost microcontroller," *Arabian J. Sci. Eng.*, vol. 38, no. 11, pp. 3059–3070, 2013.

[32] J.-K. Kang and S.-K. Sul, "Torque ripple minimization strategy for direct torque control of production motor," in *Proc. Conf. Rec. IEEE Ind. Appl. Conf.. 33rd IAS Annu. Meeting*, 1998, pp. 438–443.

[33] D. Casadei, G. Serra, A. Tani, and L. Zarri, "Assessment of direct torque control for induction motor drives," *Bull. Polish Acad. Sci., Tech. Sci.*, vol. 54, no. 3, pp. 237–254, 2006.

[34] M. Boussak and K. Jarray, "A high-performance sensorless indirect stator flux orientation control of induction motor drive," *IEEE Trans. Ind. Electron.*, vol. 53, no. 1, pp. 41–49, Feb. 2006.

[35] S.-K. Sul, *Control of Electric Machine Drive Systems*, vol. 88. Hoboken, NJ, USA: Wiley, 2011.

[36] R. Krishnan, *Electric Motor Drives: Modeling, Analysis, and Control*. London, U.K.: Pearson, 2001.

[37] V. Blasko, "Analysis of a hybrid PWM based on modified space-vector and triangle-comparison methods," *IEEE Trans. Ind. Appl.*, vol. 33, no. 3, pp. 756–764, May/Jun. 1997.

[38] K. Geethanjali, A. K. Peter, and J. Mathew, "Direct torque control of induction motor drive using tms320f28335 digital signal controller," in *Proc. IEEE Recent Adv. Intell. Comput. Syst.*, 2018, pp. 147–152.

[39] V. Semiconductors, "Optoelectronic feedback control techniques for linear and switch mode power supplies," Vishay Semiconductors, Application Note: 55, Vishay Doc. No. 83711, Tech. Rep., 2011.

Antony K. Peter (Student Member, IEEE) received the B.Tech. degree in electrical and electronics engineering from Mangalam College of Engineering, Kottayam, India, in 2010 and the M.Tech. degree in power electronics from Sree Narayana Gurukulam College of Engineering, Ernakulam, India, in 2014. He is currently working toward the Ph.D. degree with the Department of Electrical Engineering, Government Engineering College, Thrissur, affiliated to APJ Abdul Kalam Technological University.

His research interests include power converters and motor drives.

Jaison Mathew (Senior Member, IEEE) received the B.Tech. degree in electrical engineering from Rajiv Gandhi Institute of Technology, Kottayam, India, in 1998, the M.Tech. degree in power systems from the College of Engineering Trivandrum, Trivandrum, India, in 2001, and the Ph.D. degree in power electronics from Indian Institute of Science, Bangalore, India, in 2014.

He is a faculty with the Department of Electrical Engineering, Government Engineering College, Thrissur, India. His research interests include multilevel inverters, motor drives, and power quality.

K. Gopakumar (Fellow, IEEE) received the B.E., M.Sc. (Engg.), and Ph.D. degrees in electrical engineering from the Indian Institute of Science, Bangalore, India, in 1980, 1984, and 1994, respectively.

He was with the Indian Space Research Organization, Bangalore, India, from 1984 to 1987. He is currently a Professor with the Department of Electronic Systems Engineering, Indian Institute of Science. His research interests include PWM converters and high power drives.

Dr. Gopakumar is a Fellow of Institution of Electrical and Telecommunication Engineers, India and Indian National Academy of Engineers. He is currently a Co-Editor in Chief for the IEEE TRANSACTION ON INDUSTRIAL ELECTRONICS and also a Distinguished Lecturer of IEEE Industrial Electronics Society (IES). He is also the recipient of the IEEE-IES Dr.-Ing. Eugene Mittelmann achievement Award-2019.